Numerical Studies of Wake Excitation in Plasma Channels*

B. A. Shadwick and J. S. Wurtele
Department of Physics, UC Berkeley and Center for Beam Physics, LBNL, Berkeley CA, USA

Abstract

The wake fields produced by an intense, short laser pulse propagating in a plasma channel with an arbitrary density profile is investigated. Plasma channels, viewed as accelerating structures, have many desirable features that are not shared by a homogeneous plasma. They are also becoming experimentally realizable. As part of an overall program to analyze plasma channels as accelerating structures, a new fluid simulation code has been developed with the primary purpose of producing fast tools to explore parameter space for both theoretical investigation of accelerator performance as well as the modeling and design of experiments. This code has flexible physics content, for example, the laser can either be fully resolved temporally or treated as ponderomotive force. An important feature, from the accelerator design point of view, is the capability to study beam propagation dynamics. We present preliminary results consisting of a detailed analysis of the transverse structure of the wake for a wide range of experimentally accessible channel profiles and characteristics of the corresponding accelerated beam.

1 INTRODUCTION

As accelerating structures, plasmas have the desirable ability to support extremely large gradients without experiencing the electrical breakdown which limits the gradient in conventional structures. Since this concept was first introduced, numerous configurations for particle acceleration in plasmas with uniform density have been proposed. (See Esarey *et al.* [1] for a comprehensive review of plasma accelerators concepts.) In the case of laser driven plasma accelerators, the usable accelerating length is determined by the distance over which the laser pulse maintains a high intensity. That is, the efficient use of the laser energy is limited by diffraction of the drive pulse. At very high intensities, relativistic optical guiding and self-channeling serve to limit diffraction and thereby extend the interaction length of the device. However, these mechanisms are inherently nonlinear; one would prefer not to rely on nonlinear processes for device operation.

Guiding in a pre-formed density channel gives the option to operate in a linear regime, since such guiding is not dependent on the laser intensity. The original theoretical investigation of guiding in channels, which considered the case of parabolic channels, was made by Sprangle and coworkers [2]. The field structure in a parabolic channel is similar to that in a homogeneous plasma; *i.e.*, the fields have an electrostatic character and the transverse field profile is determined by the driver profile. In contrast, the fields in a hollow channel are electromagnetic with the accelerating gradient being transversely uniform *independent* of the transverse profile of the driver and, to lowest order, the focusing fields are weak and linear. Since the original experimental work by Milchberg [3] numerous results in channels have been reported by many labs worldwide. Now that the experimental techniques for the controlled creation of channels is emerging, it is timely to begin systematic studies of the accelerating characteristics of plasma channels.

A consequence of the central advantage of a plasma accelerating structure, namely the ability to support gradients that would result in electrical breakdown in a metallic structure, is that the "wall" of the structure can exhibit a complex dynamics that must be faithfully modeled in order to determine the electrical properties of the structure.

2 CHARACTERIZING PLASMA CHANNELS

An optimized design of a plasma based accelerating structure requires the investigation of a considerable parameter space. By characterizing plasma structures in terms of various figures-of-merit, one can explore this parameter space in a systematic and controlled way using these characteristics as guide-posts. Here we outline the beginnings of such a search. For preliminary studies, we have found two quantitative characteristics to be quite informative [4–6]: Q and $[R/Q]$. Parameterizing the time dependence of the accelerating field as $E_z \sim \exp\left[-(i\,\omega+\gamma)(t-z/c)\right]$, we define the quality factor of the cavity, Q, as

$$Q = \frac{\omega}{2\gamma}\,,$$

which determines the number of electron bunches that can be accelerated. This is of interest for both reasons of efficiency as well for constraints imposed by applications (*e.g.*, interaction region physics issues in a collider).

Following conventional resonator theory, we define the figure of merit $[R/Q]$ as

$$\left[\frac{R}{Q}\right] \equiv \frac{E_z(0)^2}{\omega_m\,\mathcal{U}_m} \sim k_p\,Z_0,$$

where $E_z(0)$ is the peak accelerating gradient on axis, ω_m is the mode frequency, $\mathcal{U}_m$ is the mode energy per unit length, k_p is the plasma wavenumber, and Z_0 is the impedance of free space. (The last relation follows from dimensional analysis.) For the fundamental mode, $[R/Q]$ characterizes the energy spread imparted to the accelerated beam, whereas, for the higher-order modes, $[R/Q]$ characterizes beams instabilities [6]. In more pragmatic terms,

*Supported by the U. S. DoE under grant No. PDDEFG-03-95ER-40936.

$[R/Q]$ can be viewed as a measure of the gradient achieved ($E_z(0)$) for the energy invested in the mode ($\mathcal{U}_m$).

3 THE BASIC MODEL

We model the plasma as relativistic, cold, fluid electrons with a neutralizing, immobile ionic background. In addition, we make the following approximations: all field quantities are assumed to be quasi-static, *i.e.*, they are assumed to depend only upon $\xi = t - z/c$; the laser-plasma interaction is modeled ponderomotively; and the assumption of slab geometry. Given these approximations, the fluid momentum balance equations become

$$\left(1 - \frac{v_z}{c}\right)\frac{\partial p_x}{\partial \xi} + v_x \frac{\partial p_x}{\partial x} \;=\; q\left(E_x - \frac{v_z}{c}B_y - mc^2\frac{\partial \gamma_{\rm L}}{\partial x}\right),$$

and

$$\left(1 - \frac{v_z}{c}\right)\frac{\partial p_z}{\partial \xi} + v_x \frac{\partial p_z}{\partial x} \;=\; q\left(E_z + \frac{v_x}{c}B_y + mc\frac{\partial \gamma_{\rm L}}{\partial \xi}\right),$$

where $\gamma_{\rm L}(x,\xi) = \sqrt{1+a^2}$ and $a(x,\xi)$ is the dimensionless vector potential of the incident laser. This dimensionless vector potential is related to the vector potential by

$$\mathbf{A}_{\rm L} = \sqrt{2}\,\frac{mc^2}{q}\,a(x,\xi)\cos(\omega_0\,\xi)\,.$$

Here the fundamental variables are p_x and p_z; v_x and v_z are only a shorthand notation for $p_x/(m\gamma)$ and $p_z/(m\gamma)$, respectively. The electron density, n_e, satisfies the continuity equation:

$$\frac{\partial n_e}{\partial \xi} + \frac{\partial v_x n_e}{\partial x} - \frac{1}{c}\frac{\partial v_z n_e}{\partial \xi} = 0\,.$$

The electromagnetic fields are determined by Maxwell's equations coupled to the fluid current density ($qn_e\mathbf{v}$) and charge density (qn_e) *viz.*,

$$\frac{\partial B_y}{\partial \xi} - \frac{\partial E_x}{\partial \xi} - c\frac{\partial E_z}{\partial x} \;=\; 0\,, \qquad (1)$$

$$\frac{\partial E_x}{\partial \xi} - \frac{\partial B_y}{\partial \xi} + \frac{4\pi q}{m}\,n_e\,v_x \;=\; 0\,, \qquad (2)$$

$$\frac{\partial E_z}{\partial \xi} - c\frac{\partial B_y}{\partial x} + \frac{4\pi q}{m}\,n_e v_z \;=\; 0\,,$$

$$4\pi q(n_e - n_i) - \frac{\partial E_x}{\partial x} + \frac{1}{c}\,\frac{\partial E_z}{\partial \xi} \;=\; 0\,,$$

where n_i is the background ion density. Note that through Ampere's law, Poisson's equation and the continuity equation are equivalent and thus only one of these is required. Computationally, when solving the full non-linear system, it is advantageous to use Poisson's equation in place of the continuity equation as the former is linear whereas the latter is non-linear. In the absence of the laser driver, this system possess an invariant,

$$\mathcal{E} \;=\; mc^2\int dx\; n_e\,(\gamma-1)(1-\frac{v_z}{c}) + \frac{1}{8\pi}\int dx\left[E_z^2 + (E_x - B_y)^2\right],$$

which expresses energy balance in the moving frame. (As we will see below this interpretation is more apparent in the linearized theory.)

Numerically, it is desirable to solve the model equations in dimensionless form. Let n_0 be a characteristic plasma density; for example, the plateau value at large transverse distance from the channel. The dimensionless variables used for computation, $\widehat{\xi}$, $\widehat{x}$, $\widehat{n}_e$, $\widehat{n}_i$, $\widehat{\mathbf{p}}$, $\widehat{\mathbf{E}}$ and $\widehat{\mathbf{B}}$, are then defined by: $\omega_p\,\xi = \widehat{\xi}$, $k_p\,x = \widehat{x}$, $n_e = n_0\,\widehat{n}_e$, $n_i = n_0\,\widehat{n}_i$, $\mathbf{p} = mc\,\widehat{\mathbf{p}}$, $\mathbf{E} = (mc/q)\,\omega_p\,\widehat{\mathbf{E}}$, and $\mathbf{B} = (mc/q)\,\omega_p\,\widehat{\mathbf{B}}$. The plasma frequency, w_p, is related to n_0 in the usual way: $\omega_p^2 = (4\pi q^2/m)\,n_0$ and $k_p = \omega_p/c$.

4 LINEAR THEORY

A significant advantage of the pre-formed channel is its ability to guide a laser pulse in the *linear* regime as contrasted with the non-linear processes responsible for guiding in an initially homogeneous plasma. Motivated by the desire to operate in this linear regime, we consider the linearized fluid equations and study linear wake excitation. The linearized momentum equations are

$$\frac{\partial v_x}{\partial \xi} = E_x - \frac{1}{2}\,\frac{\partial a^2}{\partial x} \quad \text{and} \quad \frac{\partial v_z}{\partial \xi} = E_z + \frac{1}{2}\,\frac{\partial a^2}{\partial \xi}\,,$$

where we have expanded $\gamma_{\rm L}$ under the assumption of small a, which is in keeping with the premise of linear theory. In the dimensionless system, linearly there is no distinction between $\mathbf{p}$ and $\mathbf{v}$. Here we are linearizing about the quiescent state, so the density appearing in Poisson's equation is that of the perturbation. Thus, the perturbed density only couples through Poisson's equation and is therefore completely determined by the electric field. Let $n_e^{(0)}$ denote the equilibrium electron density. The linearized energy invariant

$$\mathcal{E} \;=\; \frac{1}{2}\,m\int dx\; n_e^{(0)}\,\left(v_x^2 + v_z^2\right) + \frac{1}{8\pi}\int dx\left[E_z^2 + (E_x - B_y)^2\right] \qquad (3)$$

can be understood in terms of Poynting's theorem in the quasi-static approximation:

$$\frac{\partial}{\partial \xi}\left[\frac{1}{2}\,n_e^{(0)}v^2 + \frac{1}{8\pi}\left(E^2 + B^2\right)\right] + \nabla\cdot\mathbf{S} = 0\,,$$

where the components of the Poynting flux, $\mathbf{S}$, are given by

$$S_x = -\frac{1}{4\pi}B_y\,E_x\,, \quad \text{and} \quad S_z = \frac{1}{4\pi}\,B_y\,E_x\,.$$

Combining these pieces, Poynting's theorem becomes

$$\frac{\partial}{\partial \xi}\left[\frac{1}{2}\,n_e^{(0)}\left(v_x^2 + v_z^2\right) + \frac{1}{8\pi}\left(E^2 + B^2 - 2E_x\,B_y\right)\right] - \frac{1}{4\pi}\frac{\partial B_y\,E_z}{\partial x} = 0\,.$$

Integrating this expression over x yields $\partial\mathcal{E}/\partial\xi = 0$. Hence, the invariance of $\mathcal{E}$ simply expresses conservation of energy for each ξ-slice.

5 COMPUTATIONAL METHODS

For both the linear and non-linear models, we use the Crank-Nicholson technique to discretize the relevant equations. Although this method is implicit, it has three significant advantages: it is (linearly) unconditionally stable, exhibits no amplitude dissipation, and is second-order in both x and ξ. These characteristics allow for a large ratio of the ξ to x step sizes keeping execution time down even for runs with fine spatial resolution. We take a uniform grid in both x and ξ. Let $f_j^n = f(\xi_n, x_j)$ and let $\Delta\xi$ and Δx be the x and ξ grid spacings, respectively. In this method, the equations are discretized at $(\xi_{n+1/2}, x_j)$, *i.e., between* the ξ grid-points. The ξ-derivatives are approximated as

$$\frac{\partial f}{\partial \xi}(\xi_{n+1/2}, x_j) = \frac{f_j^{n+1} - f_j^n}{\Delta\xi} + \mathcal{O}(\Delta\xi^2)\,.$$

All other quantities are evaluated at $\xi_{n+1/2}$ by averaging their values at ξ_n and ξ_{n+1}, *viz.,*

$$\frac{\partial f}{\partial x}(\xi_{n+1/2}, x_j) = \frac{f_{j+1}^{n+1} - f_{j-1}^{n+1} + f_{j-1}^{n+1} - f_{j-1}^{n}}{4\Delta x} + \mathcal{O}(\Delta\xi^2 + \Delta x^2)\,,$$

and

$$f(\xi_{n+1/2}, x_j) = \frac{1}{2}\left(f_j^{n+1} + f_j^n\right) + \mathcal{O}(\Delta\xi^2)\,.$$

Discretizing the equations between the ξ grid-points yields a finite-difference approximation that is second order in $\Delta\xi$ while only using information from *two* ξ steps. It this latter property that is responsible for the unconditional stability. Not having $\Delta\xi$ linked to Δx by a Courant condition turns out to be extremely valuable; in the linear case, we are able to obtain accurate solutions even when $\Delta\xi/\Delta x$ is quite large (~ 20), significantly reducing both storage requirements and computing time. Explicitly, the Crank-Nicholson discretization of the linear equations is

$$v_{x_j}^{n+1} - v_{x_j}^{n} - \frac{\Delta\xi}{2}\left(E_{x_j}^{n+1} + E_{x_j}^{n}\right) = 0\,,$$

$$v_{z_j}^{n+1} - v_{z_j}^{n} - \frac{\Delta\xi}{2}\left(E_{z_j}^{n+1} + E_{z_j}^{n}\right) = 0\,,$$

$$B_{y_j}^{n+1} - B_{y_j}^{n} - E_{x_j}^{n+1} + E_{x_j}^{n} - \frac{\Delta\xi}{2\Delta x}\left(E_{z_{j+1}}^{n+1} + E_{z_{j+1}}^{n} - E_{z_{j-1}}^{n+1} - E_{z_{j-1}}^{n}\right) = 0\,,$$

$$E_{x_j}^{n+1} - E_{x_j}^{n} - B_{y_j}^{n+1} + B_{y_j}^{n} + \frac{\Delta\xi}{2}\, n_e{}^{(0)}(x_j)\left(v_{x_j}^{n+1} + v_{x_j}^{n}\right) = 0\,,$$

$$E_{z_j}^{n+1} - E_{z_j}^{n} + \frac{\Delta\xi}{2}\, n_e{}^{(0)}(x_j)\left(v_{z_j}^{n+1} + v_{z_j}^{n}\right) - \frac{\Delta\xi}{2\Delta x}\left(B_{y_{j+1}}^{n+1} + B_{y_{j+1}}^{n} - B_{y_{j-1}}^{n+1} - B_{y_{j-1}}^{n}\right) = 0\,.$$

Provided that the x-grid extends a reasonable distance from the channel (so that the transverse gradients of the fields are negligible at the computational boundary), this discretization will honor the invariance of $\mathcal{E}$ nearly to machine precision *independent* of the size of $\Delta\xi$. While this can be demonstrated explicitly, it can be more simply understood. Consider first discretizing the equations in x using, say, central differences. This will yield a (large) set of coupled ODE's (in ξ) which we then solve using the mid-point rule. This procedure produces the same discretization as the Crank–Nicholson method. It is well-known that the mid-point rule will preserve exactly quadratic invariants. Hence solving these ODE's with the mid-point rule (or equivalently, solving the original PDEs with the Crank–Nicholson method) will preserve any quadratic invariants possessed by the system. Here there is a slight complication due to the transverse integration in (3) resulting in $\mathcal{E}$ being only an approximate invariant of the spatially discrete system, which is why the preservation of $\mathcal{E}$ is only nearly exact.

We take a somewhat novel approach to constructing the simulation code. Proceeding from a high-level symbolic description of the PDE's, a custom code generator produces the necessary C++ source to implement the PDE solver. Since the discretized equations are implicit, at its core, the PDE solver must solve a large block-tri-diagonal linear system. The linear system solver is implemented using templates and a traits-like mechanism is used to specify the details of the linear system corresponding to the PDE. The code generator essentially produces a specialization of the traits class describing the specific linear system. This approach strikes balance between complexity of code generator and demands placed on the compiler while still producing code equal in quality to the best hand-optimized code. This approach makes possible optimizations that would be tedious and error prone if carried out by hand. The overall effect is to raise the level of abstraction of the implementation of the PDE solver [7].

6 LINEAR RESPONSE

In the linear case, we are fundamentally interested in the plasma response to a ponderomotive impulse as it encapsulates the entire plasma behavior. By integrating the equations of motion analytically from $\xi = -\varepsilon$ to $\xi = \varepsilon$ and taking the limit $\varepsilon \to 0$ we can convert a ponderomotive impulse into initial conditions for the homogeneous equations. We assume a quiescent state for $\xi < 0$ and apply a ponderomotive impulse at $\xi = 0$. With this driver, the momentum equations become:

$$\frac{\partial v_x}{\partial \xi} = E_x - \frac{1}{2}\,\frac{\partial a^2(x)}{\partial x}\,\delta(\xi)\,,$$

and

$$\frac{\partial v_z}{\partial \xi} = E_z + \frac{1}{2}\,a^2(x)\,\delta'(\xi)\,.$$

Integrating these equations from $\xi = -\varepsilon$ to $\xi = \varepsilon$ we find

$$v_x(\varepsilon, x) = \int_0^{\varepsilon} d\xi\; E_x(\xi, x) - \frac{1}{2}\,\frac{\partial a^2(x)}{\partial x}\,,$$

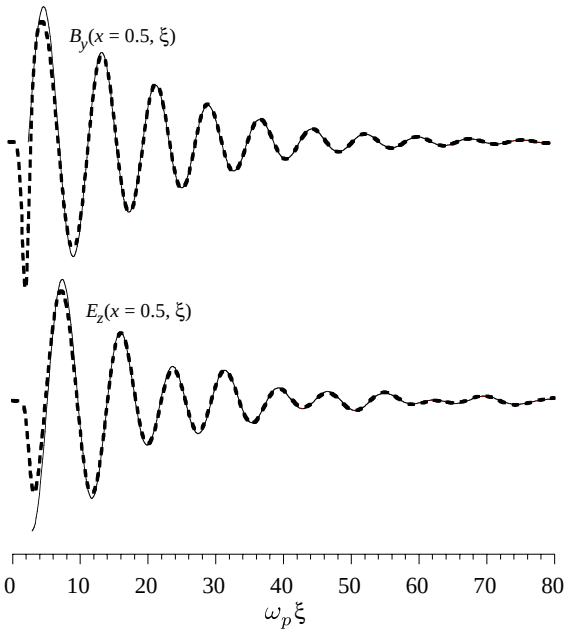

Figure 1: Comparison of the ponderomotively driven case (thick dashed line) and the response function generated from initial conditions (thin solid line) as described in the text. Here the density profile is $n_e{}^{(0)}(x) = (k_p\,x)^2$ and the driver pulse shape is $\exp(-2(\omega_p\,\xi - 2.5)^2)$. The fields are plotted at a transverse location of $k_p\,x = 0.5$.

and

$$v_z(\varepsilon, x) \;=\; \int_0^{\varepsilon} d\xi\; E_z(\xi, x)\,.$$

We expect the fields to be smooth functions for $\xi > 0$, so we may approximate the integrals as

$$\int_0^{\varepsilon} d\xi\; f(\xi) = \frac{\varepsilon}{2}\left[f(\varepsilon) + f(0^+)\right] + \mathcal{O}(\varepsilon^3)\,.$$

Taking the limit $\varepsilon \to 0^+$, gives

$$v_x(0^+, x) = -\frac{\partial a^2(x)}{\partial x} \quad \text{and} \quad v_z(0^+, x) = 0\,.$$

In the same way, (1) and (2) lead to $E_x(0^+, x) = 0$ and $B_y(0^+, x) = 0$. Lastly, by adding (1) and (2), and taking $\varepsilon \to 0^+$, we have

$$\frac{\partial Ez}{\partial x}(0^+, x) = n_e{}^{(0)}(x)\, v_x(0^+, x)\,,$$

which must then be solved to obtain $Ez(0^+, x)$. In Fig. 1, we compare the plasma response to a ponderomotive pulse having a Gaussian envelope in ξ with the response obtained using these initial conditions. Other than the initial transient (and an overall normalization), the ξ behavior of the two solutions is identical. This allows for computation of the Green's function without having to deconvolve the driver envelope or to numerically approximate a δ-function. Amongst other uses, ready access to the channel Green's function allows for efficient optimization studies [8].

7 HOLLOW CHANNELS

In the ideal hollow channel, $\omega_p(x) = \omega_{p_0}\theta(|x| - b)$, where θ is the Heavyside function. Here it is possible, in the context of linear theory, to obtain an analytical expression for the wake field [9]. In this case, one finds that the channel mode has infinite Q and oscillates at a frequency, $\omega_{\rm ch}$, which is less than ω_{p_0}. For the non-ideal case, *i.e.*, where the channel walls are not infinitely steep, matters are more complicated. The dielectric function, $\epsilon = 1 - \omega_p^2(x)/\omega^2$, is evidently spatially dependent and every $\omega < \omega_{p_0}$ is resonant with the local plasma frequency at some location in the wall. This resonant layer leads to absorption of the wake yielding a low Q. This, in turn, means a large spread in frequency space about $\omega_{\rm ch}$, exciting much of the wall. To examine these effects in detail, we parameterize the equilibrium density as shown in Fig. 2 and assume a ponderomotive impulse with a transverse pulse shape of the form

$$a^2(x) = a_0^2\, e^{-2(x_c/w_x)^2}.$$

As an example of the effects of the resonant absorption, consider a channel with $k_p b = 2$ and $\alpha = 17^\circ$. The wake field, shown in Fig. 3, has $Q \cong 7$. Resonant absorption transfers energy from the wake field to particle kinetic energy in the region of the channel wall. The velocity fields (currents) are organized in such a way that the corresponding electromagnetic fields are also spatially localized. This process results in the development of fine-scale spatial structure in the velocity and electric fields which requires high numerical resolution in the simulations.

In practice, since the laser driver extends into the bulk plasma, an electrostatic bulk mode will be excited in addition to the electromagnetic channel mode. Furthermore, separating these modes is not a simple matter, thus it is both convenient and reasonable to define an effective $[R/Q]$ as $[R/Q]_{\rm eff} = E_z(0)^2/(\omega_m\,\mathcal{U}_T)$, where $\mathcal{U}_T$ is the *total* energy in the plasma. As a result of replacing $\mathcal{U}_m$ with $\mathcal{U}_T$, the energy spent exciting the unwanted bulk mode will be reflected in a reduction in $[R/Q]_{\rm eff}$. This effect can be seen in Fig. 4, where we plot $[R/Q]_{\rm eff}$ *vs.* driver width keeping a_0^2 and $k_p\,b$ constant. (We normalize $[R/Q]_{\rm eff}$ to $k_p^2\,Z_0$.)

The physical interpretation of this result is straightforward. The channel mode is supported by surface currents in the channel walls so a very narrow driver excites the wall only a small amount, yielding a low $E_z(0)$. Conversely, a wide driver excites the wall significantly but the expo-

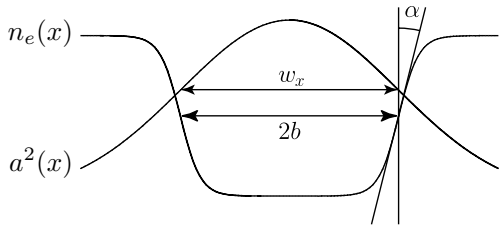

Figure 2: Density and transverse ponderomotive profiles.

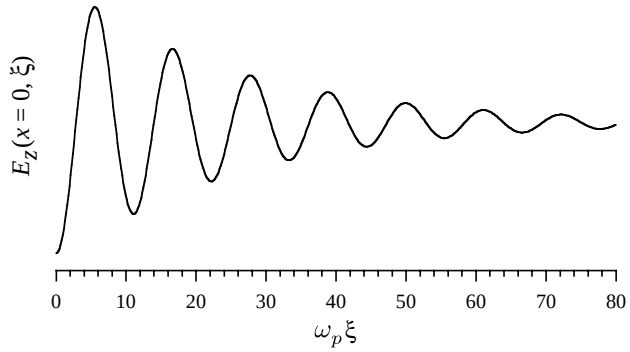

Figure 3: Longitudinal wake field on axis for a channel with $k_p b = 2$ and $\alpha = 17°$.

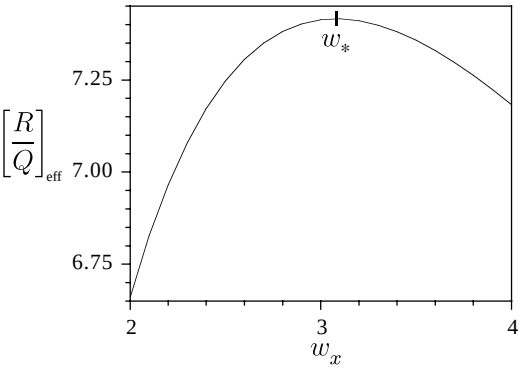

Figure 4: Effect of transverse driver width upon $[R/Q]_{\text{eff}}$. The optimal value of w_x is denoted by w_*. Here $k_p b = 2.0$ and $\tan\alpha = 0.3$

nential "wings" also excite a large bulk mode which contributes to $\mathcal{U}_T$ but not $E_z(0)$. Hence, there is an optimal driver width, w_*, which balances these competing effects. The effect of the slope of the channel walls is shown in Fig. 5. Clearly, Q is strongly dependent on this slope. As the walls are made ever less steep, the size of the resonant region grows allowing faster transfer of energy from the wake into the wall region, yielding a lower Q.

8 CONCLUSIONS

We have begun the systematic study of the accelerating properties of plasma channels by considering Q and $[R/Q]$. These figures-of-merit allow for a well defined optimization of plasma based accelerating structures. Our results are clearly preliminary; we have considered only some of the relevant parameters. In particular we have ignored the constraint on the driver width imposed by the guiding condition which may well require an operating point that differs from the optimal width determined from $[R/Q]$ considerations alone. Additionally, laboratory channels are unlikely to be completely hollow. In such channels, the base density supports an electrostatic mode in addition to the electromagnetic mode, altering the desirable beam transport properties of the hollow channel and also limiting (*via* wave breaking) the accelerating gradient that can be supported. This suggests that transverse pulse shaping (*i.e.*, a higher-order gaussian spatial mode) may prove important in the design of successful hollow channel accelerating structures.

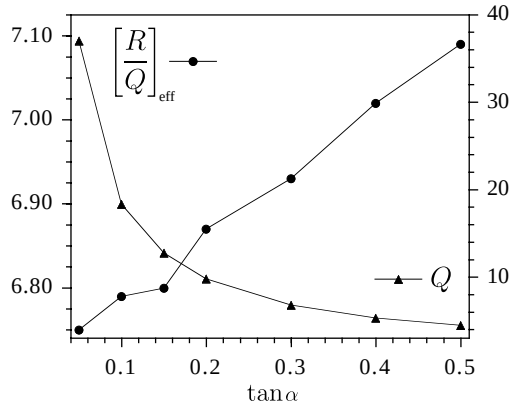

Figure 5: The effect of the wall inclination on Q and $[R/Q]_{\text{eff}}$ with optimal driver width. Here $k_p b = 2.5$

9 REFERENCES

[1] E. Esarey, P. Sprangle, J. Krall, and A. Ting, "Overview of Plasma-Based Accelerator Concepts," IEEE Trans. Plasma Sci. **24**, 252 (1996).

[2] P. Sprangle, C. M. Tang, and E. Esarey, "Relativistic Self-Focusing of Short-Pulse Radiation Beams in Plasmas," IEEE Trans. Plasma Sci. **PS-15**, 145 (1987).

[3] C. G. Durfee III and H. M. Milchberg, "Light Pipe for High Intensity Laser Pulses," Phys. Rev. Lett. **71**, 2409 (1993).

[4] B. A. Shadwick and J. S. Wurtele, "Plasma Channels as Accelerating Structures," Bull. Am. Phys. Soc. **43**, 1123 (1998).

[5] B. A. Shadwick and J. S. Wurtele, "Numerical Studies of Wake Excitation in Plasma Channels," in *Proceedings of the Sixth European Particle Accelerator Conference*, Stockholm (IOP, Bristol, 1998), pp. 827–829.

[6] C. B. Schroeder, J. S. Wurtele, and D. H. Whittum, "Multimode Analysis of the Hollow Plasma Channel Accelerator," Phys. Rev. Lett. **82**, 1177 (1999).

[7] B. A. Shadwick, "The role of automatic code generation in scientific computing," (1999), in preparation.

[8] A. Charman, B. A. Shadwick, and J. S. Wurtele, "Optimal Pulse-Shaping in the Laser Wakefield Accelerator," (1999), in preparation.

[9] T. C. Chiou, T. Katsouleas, C. Decker, W. B. Mori, G. Shvets, and J. S. Wurtele, "Laser Wake-Field Acceleration and Optical Guiding in a Hollow Plasma Channel," Phys. Plasmas **2**, 310 (1993).